

MASTER

Closed-loop density control simulations for ITER

Verhoeven, J.W.H.

Award date:
2017

[Link to publication](#)

Disclaimer

This document contains a student thesis (bachelor's or master's), as authored by a student at Eindhoven University of Technology. Student theses are made available in the TU/e repository upon obtaining the required degree. The grade received is not published on the document as presented in the repository. The required complexity or quality of research of student theses may vary by program, and the required minimum study period may vary in duration.

General rights

Copyright and moral rights for the publications made accessible in the public portal are retained by the authors and/or other copyright owners and it is a condition of accessing publications that users recognise and abide by the legal requirements associated with these rights.

- Users may download and print one copy of any publication from the public portal for the purpose of private study or research.
- You may not further distribute the material or use it for any profit-making activity or commercial gain



Faculty of Mechanical Engineering
Systems & Control group
&
Faculty of Applied Physics
Science and Technology of Nuclear Fusion group

Closed-loop density control simulations for ITER

Master Thesis

J.W.H. Verhoeven (0780966)

Supervisors:
dr. ir. F.A.A. Felici
dr. ir. P. de Vries
ir. T.C. Blanken

Eindhoven, November 2017

Abstract

Before ITER is finished important components such as the controllers, that regulate the input such that the desired behavior is achieved, are designed and tested in simulations. Incremental work on the ITER plasma density controller is continued. Models for diagnostics and observers are added. The performance of control is investigated over the full duration of an ITER discharge scenario. The simulation components are integrated into the platform for ITER control simulations, the Plasma Control System Simulation Platform (PCSSP).

A model is created to simulate the toroidal interferometer/polarimeter and the density interferometer polarimeter line-integrated density measurements. The interferometer model is extended to be used as a part of the extended kalman filter-based observer, which reconstructs the plasma density based on the measurements. With the complete simulations and the previously proposed control architecture, the system works well as the controller is capable of keeping the density between its stability limits and it is capable of ensuring a small error during the L-H and H-L mode transitions, where the error is important. A simple model of the measurement error does not have a significant impact of control performance. The work demonstrates that PCSSP can be used in practice for assessment of the density control performance for ITER.

Contents

Contents	v
1 Introduction	1
2 Model derivation	5
2.1 Models of the ITER density evolution	5
2.1.1 A control-oriented model of the evolution of plasma density in ITER	5
2.1.2 Actuator models for pellet and gas injection	9
2.2 Control solution	9
2.2.1 Iterative Learning Control	10
2.3 Extended Kalman Filter-based State Observer	11
3 Interferometer diagnostic model	13
3.1 Theory of plasma electron density measurements with interferometry	13
3.1.1 Dispersion Interferometer	13
3.1.2 Toroidal Interferometer/Polarimeter	14
3.2 Implementation of the interferometer model in MATLAB	14
3.2.1 Derivative of electron density measurements with respect to the density state variable	15
3.2.2 Concluding remarks	16
4 Control assesment	17
4.1 ITER D-T burning plasma discharge scenario	17
4.2 Control performance comparison of plasma scenario with previous work	19
4.3 Effects of including sensor and observer models	19
4.3.1 Full shot simulation with sensors and observer	20
4.3.2 Simulation of measurement errors and effect on control	22
4.4 Control assesment results	23
4.4.1 Comparison of tracking with a simple feedforward and with ILC	23
4.4.2 Comparison of tracking during L-H transition for different ILC optimisation times	24
4.4.3 Comparison of tracking during the L-H transition for different ILC costs . .	25
4.4.4 Comparison of tracking during the L-H transition with different pellet sizes	27
4.4.5 Ideal controller performance	28
5 Conclusions	29
5.1 Conclusions	29
5.2 Discussion and outlook	30
5.2.1 Sensors	30
5.2.2 Parameters	30
5.2.3 Observer and feedforward model mismatch	30
5.2.4 ITER reference plasma discharge	31

5.3	Future work	31
5.3.1	Sensor models	31
5.3.2	Termination scenario's	31
5.3.3	Hybrid control	31
5.3.4	Profile and mixed species control	32
Bibliography		33
Appendix		35
5.4	Using PCSSP	35
5.5	Linking PCSSP and IMAS	35

Chapter 1

Introduction

With the recent public attention towards addressing global warming, and considering the inevitable scarcity of fossile fuels, the need for a clean energy source is more apparent than ever. In order to adress the growing demand for energy, while transitioning to a fully green energy supply, developments in clean energy technologies are needed.

A possible solution to this energy problem comes from nuclear fusion. In a nuclear fusion reactor, atoms are heated to such temperatures that they have enough energy to overcome their repulsive forces and fuse together. The binding energy of the reaction products is lower than the binding energy of the reagents. This difference in energy is released as heat in the fusion reaction. Nuclear fusion is the process that powers the sun and other stars.

In the core of the sun the high temperature required for fusion is the results of the gravitational pressure. On earth a different solution is needed. In devices like tokamaks and stellarators, induction, electro-magnetic waves and high energy particle beams are used to heat the fuel, the hydrogen isotopes deuterium and tritium, to a hundred million degrees. The high temperature causes atoms to release their electrons, ionizing them. The partially or fully ionized particles are called a plasma. Large magnetic field coils are used to create a toroidal magnetic field in the donut shaped vessel of the tokamak and a current is driven in the plasma creating a poloidal magnetic field. Combined these leads to a helical toroidal field as indicated in figure 1.1. The magnetic and electric fields are created such that the forces generated confine the plasma, keeping it from touching the walls. If one of the many operational limits, such as the limit on maximal density, is exceeded the plasma disrupts. When this happens the plasma rapidly cools down, loses its ability to conduct current, and loses confinement. The energy, both thermal and electric, is deposited

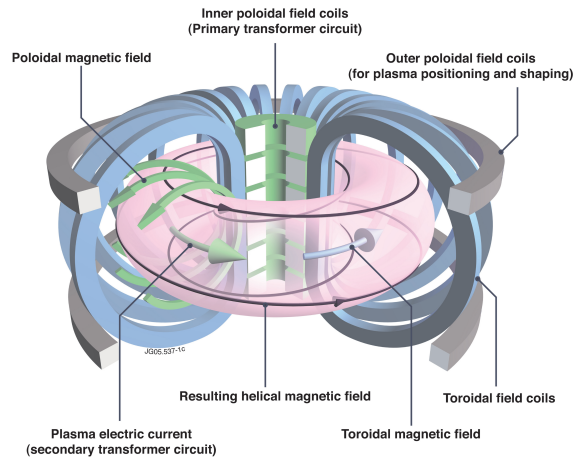


Figure 1.1: Image of the helical magnetic field inside a tokamak. Source : EUROfusion

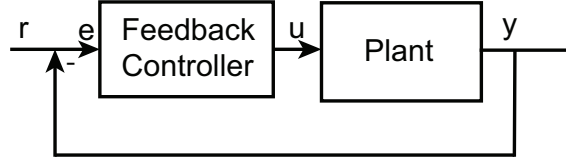


Figure 1.2: Schematic of feedback control. The output variable y is subtracted from the reference r to determine the error. The feedback controller calculates the input u to the plant, the system to be controlled, based on the error.

from the plasma into the device, which can cause damage.

In a tokamak under the right circumstances with enough heating power the plasma can transition from its normal low confinement mode (L-mode) to a high confinement mode (H-mode). In H-mode the radial transport of particles and energy is inhibited near the edge creating an edge transport barrier (ETB). Because of the better confinement in H-mode the central pressure rises and fusion conditions are more easily achieved. The transition into H-mode occurs only when the parameters such as the plasma density are within a specific range when additional heating power is turned on.

Controllers are used to ensure that certain parameters do not deviate too much from their prescribed values. Feedback controllers achieve this by comparing a measurement of the parameter with the reference value. The error, the difference between the measurement and reference, is used by the controller to determine the input signal which reduces the error. To do this a controller is created to stabilize, ensure it is always able to eventually eliminate the error, a specific system.

The ITER, latin for "the way", tokamak is currently under construction in Cadarache, France, and will be the largest tokamak to date. It is designed to do research on a burning plasma, a plasma in which the energy produced by fusion significantly contributes to maintaining its fusion conditions. Because of its size, disruptions could cause serious damage to the machine and have to be avoided as much as possible. Therefore the controllers for the various systems, such as the plasma density and temperature but also the magnetic coil currents, are designed beforehand. Because the device is not operational, models and simulations are used to create and test the controllers. Because of the complexity of the device and physics involved in fusion, many codes are used to model various parts of the system in varying degrees of detail. The Integrated Modelling and Analysis Suite (IMAS) allows for more easy communication between various codes by standardizing the input and output formats with the IMAS Data Structure (IDS) [17]. The Plasma Control System Simulation Platform (PCSSP) is a Simulink® [1] environment designed to simulate and test the controllers that make up the Plasma Control System (PCS), both individually and combined [13] [4]. Using the PCSSP and IMAS platforms allows for easy integrated modelling in which different codes for the various specific systems are used together to model the complex physics in fusion research.

One of the systems needed in early operation of ITER is the plasma electron density controller. The controller decides, based on measurements of the plasma density, when the actuators should be used to put more particles into the system to ensure the plasma density remains close to the desired or reference density. This is important because when the density becomes too low neutral beams and fuelling pellets could penetrate through the plasma and damage the machine. When the density becomes too high the Greenwald density limit could be exceeded causing a disruption. Because the capabilities of actuators and sensors available on tokamaks are limited the control problem is difficult. Moreover the complex non-linear dynamics of density evolution inside a fusion plasma change during the various parts of a plasma discharge. This calls for advanced control techniques.

In control state observers are used to estimate the state of the system based on measurements of the system output. From this state estimation physics variables that cannot be directly measured can be used as control variables. Additionally, using multiple diagnostic measurements makes the control less sensitive to measurement errors and diagnostic failure.

During previous work [15] on ITER density control, models were produced for the density evolution in the tokamak, the actuators and the controller. Models of measurement systems, such as the interferometer systems designed for density control, were not included in these simulations. Previous work has focussed on the ramp-up. This is the first stage of plasma operation during which the plasma is created and the plasma parameters such as plasma current and density increased until their desired values are reached. The following phases, flat-top and ramp-down, have not been considered. In this work models for the diagnostics and the observer, which produces an estimate of the control variable based on measurements, are added to close the control loop and the control performance is evaluated during a full plasma shot. Additionally work is done on the integration with IMAS and PCSSP.

Problem statement

The aim of this project is to advance the density control project for ITER by adding sensor models to the simulations and closing the loop by integrating a state observer. The models are implemented in the plasma control system simulation platform (PCSSP). The whole loop is then used to evaluate the performance of the controller and evaluate the influence of adding sensor and observer models to the loop. The following research questions are defined:

- What is the effect of adding more complex models for actuators, sensors, plasma physics and observers to the density control loop on controller performance?
- What is the best achievable performance of the density control loop in terms of reference tracking?
- Are the present versions of IMAS and PCSSP adequate for closed-loop density simulations of ITER?

Method

As a starting point for this project the existing simulation components are put into the PCSSP. Simulations are run on a full representative ITER H-mode shot and the developed tools for feedforward control are applied. A schematic overview of the simulation is presented in figure 1.3

The simulations are expanded with models for the diagnostics and a model for the state observer is included, as can be seen in figure 1.4

In the second chapter the used models for the density evolution, control and observer, obtained from previous work, are discussed. Chapter 3 discusses the added diagnostics and their implementation. Chapter 4 shows the results of the control simulations with the new additions. Chapter 5 contains the conclusions and discussion of this thesis. In appendix A the use of PCSSP is discussed.

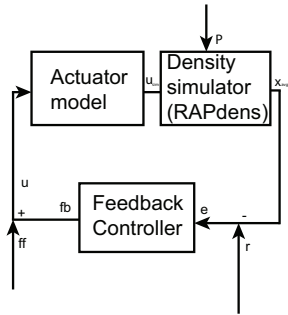


Figure 1.3: Schematic overview of the simulation components present in previous work. The plant consists of models for the gas and pellet injection systems and the electron density transport model RAPdens.

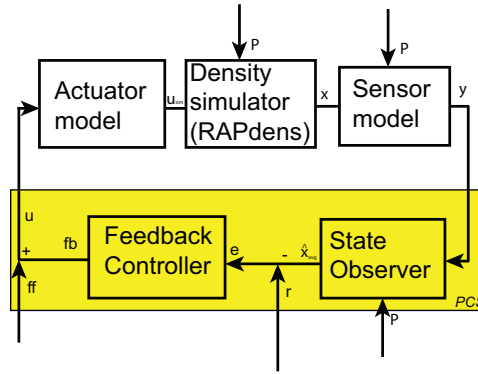


Figure 1.4: Schematic overview of the complete simulations. Sensor models for the interferometer is added to the plant, and a state observer, which contains its own synthetic diagnostic, is added to the PCS side.

Chapter 2

Model derivation

In this chapter the models that were already available from previous work on density control are discussed. First, a control oriented model for density profile evolution is discussed, followed by the simple models for the gas valve and pellet injection system. Then the control methods are discussed, and finally the state observer.

2.1 Models of the ITER density evolution

2.1.1 A control-oriented model of the evolution of plasma density in ITER

In a tokamak particles gyrate in the helical magnetic field as they follow the field lines. Because particle transport along the fieldlines is much faster than perpendicular to it, they remain in their flux surface as they move toroidally and poloidally around the tokamak. The shape and location of the flux surfaces depends on the combination of magnetic fields imposed by external magnetic coils and current profile, but because transport inside the surface is much faster than across it, the plasma parameters, such as density and temperature, are assumed to be constant within a surface. With this assumption radial transport can be considered as transport between these flux surfaces. The flux label, ρ indicated in figure 2.1, is defined as the normalized toroidal flux, such that $\rho = 0$ corresponds to the center of the plasma and $\rho = 1$ at the last closed flux surface (LCFS), the outer most flux surface whose fieldlines do not impact the walls.

A control oriented density model was created for control tools design, initially tested on the TCV and ASDEX-Upgrade tokamaks [6]. In this model the complex dynamics are modelled in a simple way. This allows for fast computation which is a requirement in control models. This density evolution model, called RAPdens, consists of a 1-D model for radial electron density evolution coupled to two 0-D equations for the wall and vacuum inventory.

In figure 2.2 a schematic representation of the density model is presented. Particles are introduced into the system via the gas valve and the pellet injection system. Particles exit the system via the cryopumps. The particles inside the system are either part of the plasma, part of the vacuum inventory, the neutral gas inside the vacuum vessel, or are part of the wall inventory, having bonded with the elements in the wall. Transport of particles between these inventories is governed by ionisation and recombination, between vacuum inventory and plasma, and absorption and release, between wall and vacuum inventories.

Plasma particle sources and sinks

There are three sources of particles in the model: the gas valves, the pellets and the Neutral Beam Injection (NBI). The gas valve is used to puff neutral gas into the vacuum vessel. This is added to

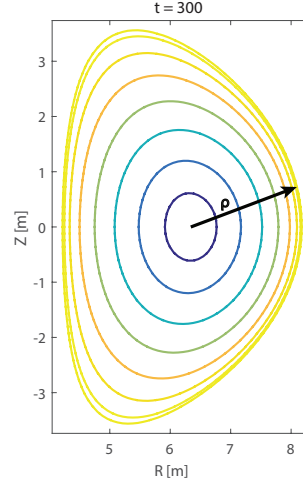


Figure 2.1: Cross section of an ITER plasma during flattop with surfaces of constant flux indicated.

the neutral vacuum inventory. The pellets are small pieces of frozen material. These are shot into the plasma at velocities of up to 500 m/s [16]. When it penetrates far enough into the plasma, the temperature of the plasma causes the pellets to ablate, turning the frozen material into gas which is ionized and becomes part of the plasma. This is modelled by placing the particles in the pellets in an area around the deposition location. In reality the deposition location is a function of the plasma temperature, pellet size and pellet velocity. In the model it is a fixed location. NBI inject neutral particles with higher energy than those in the plasma into the plasma at high velocity. This is a source of heating and current drive but also delivers particles into the plasma. It is modelled similarly to the pellet injection system, placing the particles in a small region inside the plasma. For a large device such as ITER, the fuelling capacity of the NBI system is small and therefore in this work the NBI is not considered for use in density control.

The only sinks in the system are the cryopumps that capture the neutral gas in the divertor. This is modelled by taking away part of the vacuum inventory. The cryopumps are not considered as actuators for the density control and their pumping speed is maintained fixed during operation. Therefore the actuators in the system can only add particles to the system complicating the control task.

Density transport

The evolution of the electron density, n_e , in the model is governed by diffusion and the magnetic pinch. The partial differential equation describing this density evolution is derived from a particle balance and is given by

$$\frac{1}{V} \frac{\partial}{\partial t} (n_e V') + \frac{1}{V'} \frac{\partial \Gamma}{\partial \rho} = S \quad (2.1)$$

with V the plasma volume enclosed by a flux surface, ρ the normalized toroidal flux, $V' = \delta V / \delta \rho$, S the particle sources and Γ the radial particle flux. This Γ is given by

$$\Gamma = -V' (G_1 \chi \frac{\partial n_e}{\partial \rho} + G_2 \nu n_e) \quad (2.2)$$

G_1 and G_2 are profiles and a function of the plasma geometry but in this work they are assumed to be 1. The parameters ν and χ are radial functions defining the pinch and diffusion respectively. Values for these parameters are unknown and therefore they are tuned to have the density profile match expectations based on density profiles in present day machines. χ and ν are given in figure 2.3

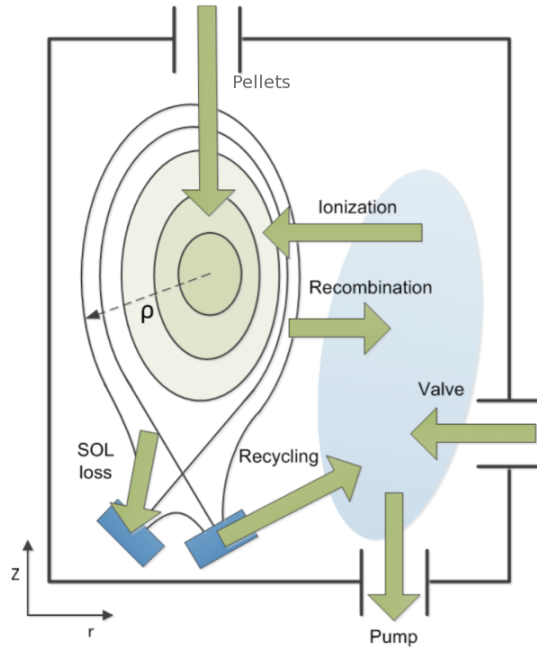


Figure 2.2: Schematic overview of the density models. Valve and pellets are sources in the system and the pumps are the sinks. Arrows indicate the processes that govern transport between the plasma, vacuum inventory and the wall inventory. [7]

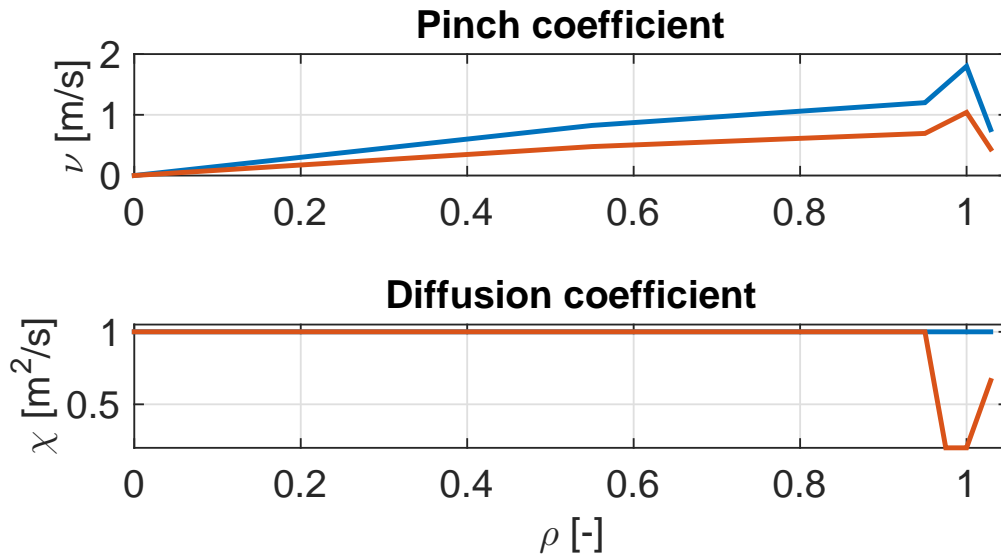


Figure 2.3: Profiles for χ and ν as a function of the normalized flux label ρ . Values for L-mode (blue) and H-mode (red) are shown. At $\rho = 1$ $\chi = 0.06 \text{ m}^2/\text{s}$ in H-mode.

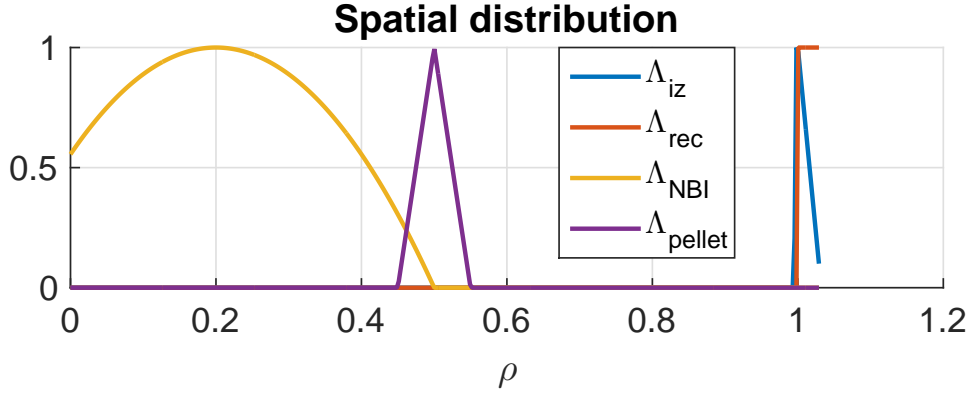


Figure 2.4: Spatial distribution for the source terms in the model

When the plasma is in H-mode the parameters for the ν and χ parameters change to match the higher confinement. The new density profile shows a clear pedestal as a result of the edge transport barrier of the H-mode. During H-mode also the pumping speed is changed to reflect the increase in pumping speed efficiency. The source terms in equation 2.1 take the form

$$S_i = \Lambda_i(\rho)\Gamma_i(t) \quad (2.3)$$

with Γ the particle flux and Λ the spatial distribution and the index i indicates the various sources and sinks. The spatial distributions are shown in figure 2.4. While these spatial distributions are a function of plasma parameters such as the plasma temperature and density, they are fixed values in the used model. More information on the sources and their particle fluxes can be found in [6]

Finally, PDE (2.1) is approximated by a set of discrete ODE's using a finite element method, with cubic spline as the basis functions and test functions resulting in

$$x_{k+1} = f(x_k, p_k) + B(p_k)u_k \quad (2.4)$$

, with p_k the external plasma parameters, u_k the input $u_k = [\Gamma_{gas}, \Gamma_{NBI}, \Gamma_{pellet}]^T$, and x_k the state vector

$$x_k = \begin{pmatrix} b(t_k) \\ N_w(t_k) \\ N_v(t_k) \end{pmatrix} \quad (2.5)$$

$b(t_k)$ are the spline coefficients. The density profiles $n(\rho, t)$ can be calculated using

$$n(\rho, t) = \Lambda(\rho)b(t). \quad (2.6)$$

The external parameter input p_k is defined as

$$p_k = [c_D \ c_H \ T_{e,b} \ I_p \ V \ V' \ \kappa \ A \ p \ G_1 \ G_0] \quad (2.7)$$

with c_D and c_H variables indicating whether the plasma is diverted and in H-mode respectively, $T_{e,b} = T_{e,\rho=1}$ is the electron temperature at the last closed flux surface, I_p is the total plasma current, V the total plasma volume, V' the time derivative of the total plasma volume, κ the elongation at the LCFS, A the plasma cross section, G_1 and G_2 functions of the plasma geometry and p a variable indicating if the plasma has been formed. The parameters G_1 and G_2 are assumed to be 1 for now corresponding to a circular plasma. The parameters data is obtained from a reference plasma discharge simulation, which is described in chapter 4. Later all the plasma parameters will come from real-time equilibrium reconstruction.

2.1.2 Actuator models for pellet and gas injection

The gas and pellet injection systems are modelled as follows:

Gas Injection System (GIS)

The gas injection system consists of long pipes with Mass Flow Control (MFC) valves. The length of pipes is in the order of 20 and more meters which results in a delay between opening the valves and the gas entering the vacuum vessel ranging between half a second and more than one second based on the gas species and flow. This is modelled using a 1st order transfer function

$$u_k = \frac{1}{\tau s + 1} \quad (2.8)$$

As a result of the long time constant, a significant feedforward contribution in the control solution is expected in particular during the initial phase of the discharge [15].

The maximum gas fuelling is set to 200 particles per second.

Pellet injection system (PIS)

The pellet injectors can shoot pellets of four different sizes into the plasma. The deposition location of the pellets is a function of the plasma temperature and density, the pellet size and the injection velocity. In the density model, this dependency is not taken into account and the deposition location is fixed. The smaller 17 and 33 cubic mm pellets cannot penetrate far into the plasma during most of the plasma operation and are mostly intended for edge localized mode (ELM) control [5]. Therefore only the two largest pellets of 50 and 92 cubic mm are considered for density control [16].

Because of the discrete quantity of material delivered by a single pellet, the developed model integrates the request from the controller until the size of a single pellet is reached. Then the pellet is triggered and the pre-defined quantity of material is deposited in the specific plasma region. The large 92 cubic mm pellets contain approximately 6×10^{21} atoms. With a maximal injection frequency of 16 Hz the maximal fuelling rate is approximately 9.6×10^{22} particles per second.

Because the pellet penetration depth is a function of the plasma density and temperature, using pellet injection before the plasma is sufficiently dense, the pellets will not ablate and impact the other side of the torus, potentially damaging the wall. Therefore the PIS cannot be used before the core density has surpassed the minimum density value n_0 ;

Switching actuators

Because the gas injection is slow, and at high temperatures the ionization depth becomes too small for effective fuelling using the GIS, pellet fuelling is required from a certain point during the discharge. The PIS cannot be used in the beginning and so at some point during the shot the control has to switch from using the gas injection to using pellet injection as the actuator. In reality this is a function of plasma density and temperature. In this work it is modelled with a timer, switching the feedback control from gas injection to pellets at $t = 10s$.

2.2 Control solution

In figure 1.4 the control loop is displayed, with e the control error, x the density state, y the measurement related to the plasma density, \hat{y} the estimated measurement, r the density reference and \hat{x} the estimated density state. The transfer function for the feedback controller C is synthesized using robust control techniques. It is a Single Input Single Output (SISO) transfer function with the error on volume average density as input and gives a number of particles to be injected per second as output. Using a model of the plant linearised around a point halfway during ramp-up

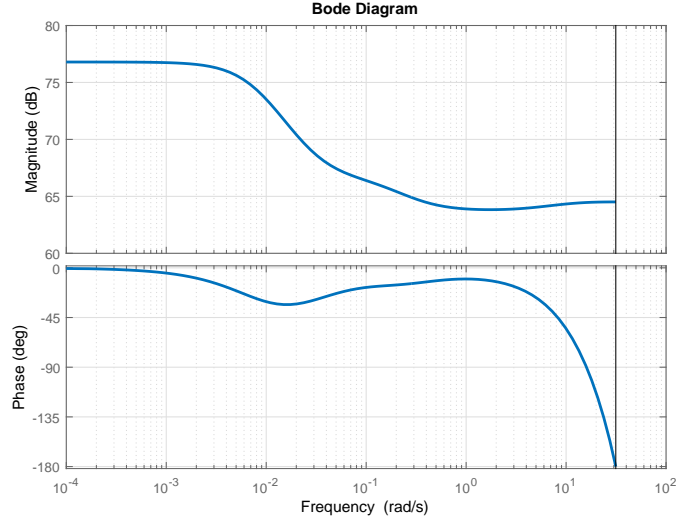


Figure 2.5: Bode diagram of the feedback controller showing the magnitude and phase response as a function of input signal frequency.

an algorithm creates the controller which guarantees stability in a parameter space around the chosen work point. A 12th order feedback controller is synthesized in [15] which is used in this work. The bode diagram detailing the controller is shown in figure 2.5.

For performance feedforward control is needed. The feedforward waveform is created using an iterative learning control (ILC) algorithm. The feedback controller is only required for stability. The requirements for the control solution are different during ramp-up, flatterp and ramp-down. During ramp-up a strong feedforward is required to achieve performance with the slow actuators. Considering the transition to H-mode and the changing dynamics, the tracking error during the requirements on the size of the tracking error are not the constant during ramp-up. Combined with the feedforward, a weak feedback control is preferable. During flatterp phase, the feedforward is not required for performance and feedback can be used to ensure good tracking behavior. Because of the different requirements for feedback control during ramp-up and flatterp a different controller is used. During the ramp-up phase, a gain with $P = -20dB$ is added to the controller presented in 2.5. During the rest of the shot, the controller presented in 2.5 is used without additions. Switching the controller makes this a hybrid system.

This control architecture was proposed considering only ramp-up. During the simulations of a full shot a feedforward waveform for various parts of the shot is considered.

2.2.1 Iterative Learning Control

In iterative learning control repeated experiments are used to tune the feedforward waveform to an optimal state [20]. An optimal feedforward waveform is determined by minimizing a cost function. The cost function for the used ILC algorithm includes four cost terms

- control error integrated over the duration of the shot, $\|W_e \vec{e}^{j+1}\|_2^2$
- control effort integrated over the duration of the shot, $\|W_u \partial \vec{u}^{j+1} - \vec{u}^j\|_2^2$
- change of input signal values with respect to the feedforward waveform used in the previous iteration of the ILC, $\|W_{\Delta u} \partial \vec{u}^{j+1} - \vec{u}^j\|_2^2$
- control error during certain phase of the shot, $\|W_{LH} \vec{e}^{j+1}\|_2^2$,

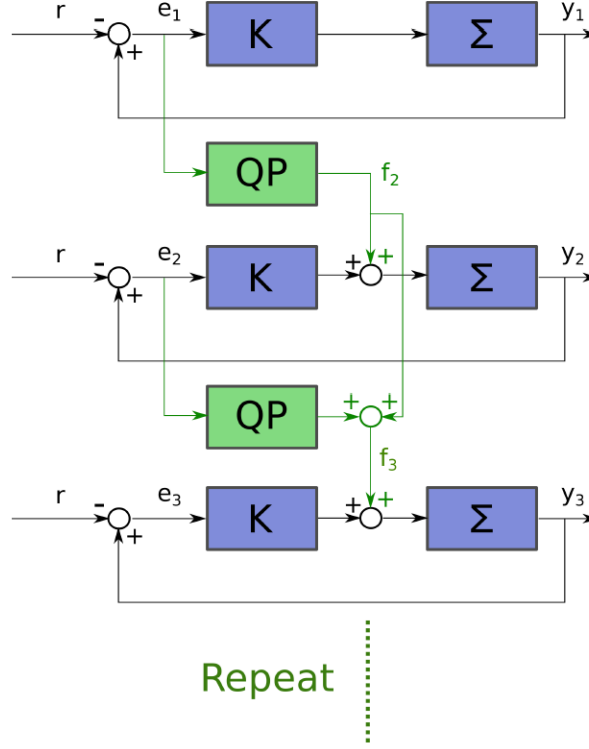


Figure 2.6: Schematic overview of the ILC algorithm. The simulation is run and the error signal e is used as input for the Quadratic Programming (QP) cost function to calculate the feedforward signal f for the next simulation. [15]

With the final cost only applying on errors around the time of the L-H transition. Because no experiments can be done at this moment, simulations using different parameters and dynamics are used to create the experiments needed in the algorithm.

The algorithm has three steps

1. run initial simulation with a first guess for a feedforward waveform
2. use the linearized model to calculate optimal variations on the feedforward waveform
3. test new feedforward waveform in a new experiment

Steps 2 and 3 are repeated a number of times to iterate to a final value.

2.3 Extended Kalman Filter-based State Observer

An observer is used to reconstruct a controlled state variable from measurements which can be indirect and erroneous. A extended kalman filter (EKF) based observer for plasma density has been designed and tested on TCV [7]. In this project, the observer is implemented in the ITER density control loop simulation.

The extended kalman filter [14] creates a predicted state estimate

$$\hat{x}_{k|k-1} = f(\hat{x}_{k-1|k-1}, u_{k-1}), \quad (2.9)$$

at based on the evolution of the previous state estimate $\hat{x}_{k-1|k-1}$ and input u_{k-1} , and a predicted covariance estimate

$$P_{k|k-1} = F_{k-1}P_{k-1|k-1}F_{k-1}^\top + Q_{k-1}, \quad (2.10)$$

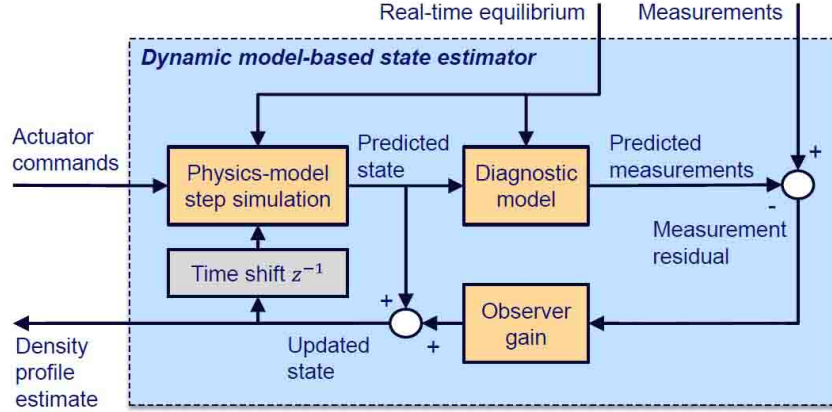


Figure 2.7: Schematic of EKF components. Source: [7].

with Q the covariance matrix and the state transition matrix

$$F_{k-1} = \frac{\partial f}{\partial x} \big|_{\hat{x}_{k-1|k-1}, u_{k-1}}. \quad (2.11)$$

Then an update to the state estimate and covariance estimate based on the measurements of the system,

$$z_k = h(x_k), \quad (2.12)$$

is computed. First the innovation residual,

$$y_k = z_k - h(\hat{x}_{k|k-1}), \quad (2.13)$$

and the innovation covariance,

$$S_k = H_k P_{k|k-1} H_k^\top + R_k, \quad (2.14)$$

with z_k the measurements, R_k the measurement covariance and

$$H_k = \frac{\partial h}{\partial x} \big|_{\hat{x}_{k-1|k-1}}. \quad (2.15)$$

The near-optimal Kalman gain is:

$$K_k = P_{k|k-1} H_k^\top S_k^{-1}. \quad (2.16)$$

Finally the update step is completed with the updated state estimate,

$$\hat{x}_{k|k} = \hat{x}_{k|k-1} + K_k y_k, \quad (2.17)$$

and the updated covariance matrix,

$$P_{k|k} = (I - K_k H_k) P_{k|k-1}. \quad (2.18)$$

The observer uses the RAPdens model for its internal density estimate, f . Model parameters are changed between the density model used as the plant simulator and the model used in the EKF to simulate the modelling errors in the observer model. The observer inputs R , the covariance of the measured signal, and Q , the covariance of the model uncertainty are set to $10^{-3} \times I$, with I the identity matrix. The observer requires not only an predicted measurement, but also H_k a derivative of the measurement with respect to the density input signal, which is to be provided by the synthetic diagnostic module.

Chapter 3

Interferometer diagnostic model

The characteristics of the diagnostic systems determine the output signals available for feedback control. It is important to model the diagnostic devices to simulate the information as it is available in the actual device to ensure the simulation mimics the actual system as closely as possible. In this chapter the diagnostic models for the interferometers and their implementation are discussed.

3.1 Theory of plasma electron density measurements with interferometry

Interferometry is one of the ways to measure plasma density in a tokamak. The measurement is based on a correlation between the phase propagation speed and plasma density. In principle two laser beams are sent out on paths of equal length. One of the beams travels through the plasma, and due to the difference in phase propagation speed between vacuum and plasma a phase difference between the two beams is created. This phase difference is given in (3.1).

$$\phi_p = \frac{2\pi}{\lambda} \int N(I) dl \quad (3.1)$$

with λ the laser wavelength in vacuum and $N(I)$ the refractive index along the chord. The refractive index is defined in 3.2.

$$N = \sqrt{1 - \frac{\omega^2}{\omega_{pe}^2}} \quad (3.2)$$

$\omega = \frac{2\pi c}{\lambda}$ with c the speed of light. The plasma frequency relates to the density as:

$$\omega_{pe}^2 = \frac{n_e e^2}{\epsilon_0 m_e \gamma} \quad (3.3)$$

with n_e the electron density, e the electrons charge, $m_e \gamma$ the relativistic electron mass and ϵ_0 the permittivity of vacuum. Because the phase difference is proportional to the plasma density, the line-integrated plasma density can be calculated from the measurement. To get a line-averaged measurement the phase difference is divided by the length of the path. Because the plasma density is not uniformly distributed, commonly multiple beams are used to reconstruct the density profile. For ITER two of the main interferometry systems for density control are the dispersion interferometer (DI) [3] and the two-color Toroidal Interferometer/Polarimeter(TIP) [8].

3.1.1 Dispersion Interferometer

The Dispersion interferometer has two chords, one radial and one tangential to the plasma. The wavelength of the system is chosen such that fringe jumps, a common issue with interferometers which occurs when the phase difference changes more than 2π between subsequent samples, do not occur. This is because the entire expected measurement range should fall in one fringe,.

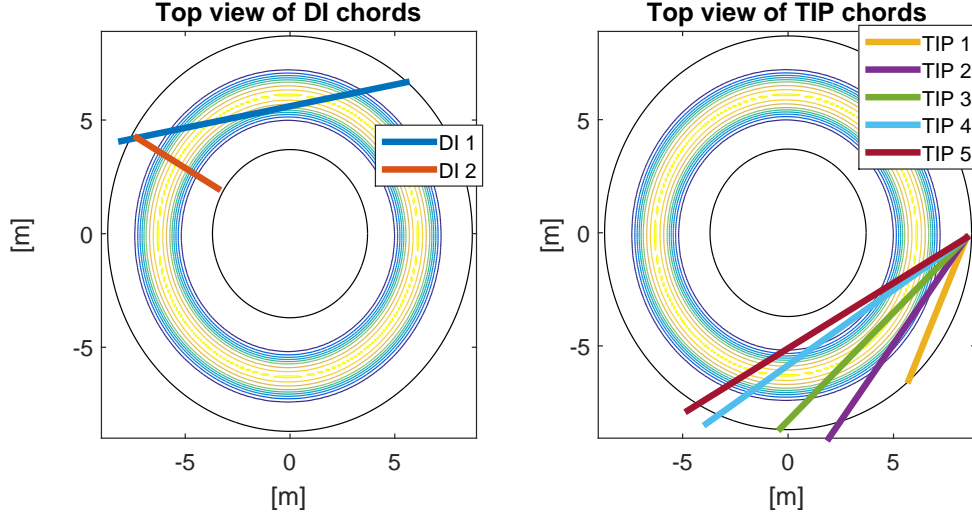


Figure 3.1: Schematic top view with interferometer chords indicated for the DI (left) and TIP (right)

3.1.2 Toroidal Interferometer/Polarimeter

The two-color Toroidal Interferometer/Polarimeter has five chords, tangential to the plasma. From this a radial density profile can be constructed. The interferometer uses two parallel lasers of different color for eliminating vibrations. The polarimeter measures the phase rotation of the beam which provides a coarse absolute measurement of the density and is expected to be used to correct for fringe jumps in more precise interferometer measurements.

3.2 Implementation of the interferometer model in MATLAB

An interferometer model, provided at ITER, is implemented in simulink to represent the DI and TIP systems. Because this model is fairly straightforward and does not take into account some of the more complicated physics it functions for both systems.

The code requires besides the density profile, the electron temperature profile to calculate the relativistic electron mass and the 2D flux map as inputs. During operation these would be available from realtime equilibrium solvers and other diagnostics. For each chord the model calculates the line averaged measurement by dividing the chord into n sections. For each section the local flux value is interpolated and with that the local electron temperature and density are found and the resulting phase change is calculated. The phase changes are summed for each chord and this integrated phase difference is provided as the output measurement.

The line-averaged density, which is the quantity used in the control and observer, is calculated from this phase difference output at the end of the model. The interferometer gives out a line-averaged density. The synthetic diagnostic code divides the chord into many small pieces and calculates the local refractive index. The line-averaged density then becomes :

$$n_{la} = \frac{\epsilon_0 m_e 4\pi}{e^2 L \lambda} \sum N(I)_p L_p \quad (3.4)$$

with L the length of the chord and L_p the length of a chord section.

Taking n chord measurements from one or more diagnostics the measurement input h is defined as:

$$h = [n_{la,1}, n_{la,2}, \dots, n_{la,n}]^T \quad (3.5)$$

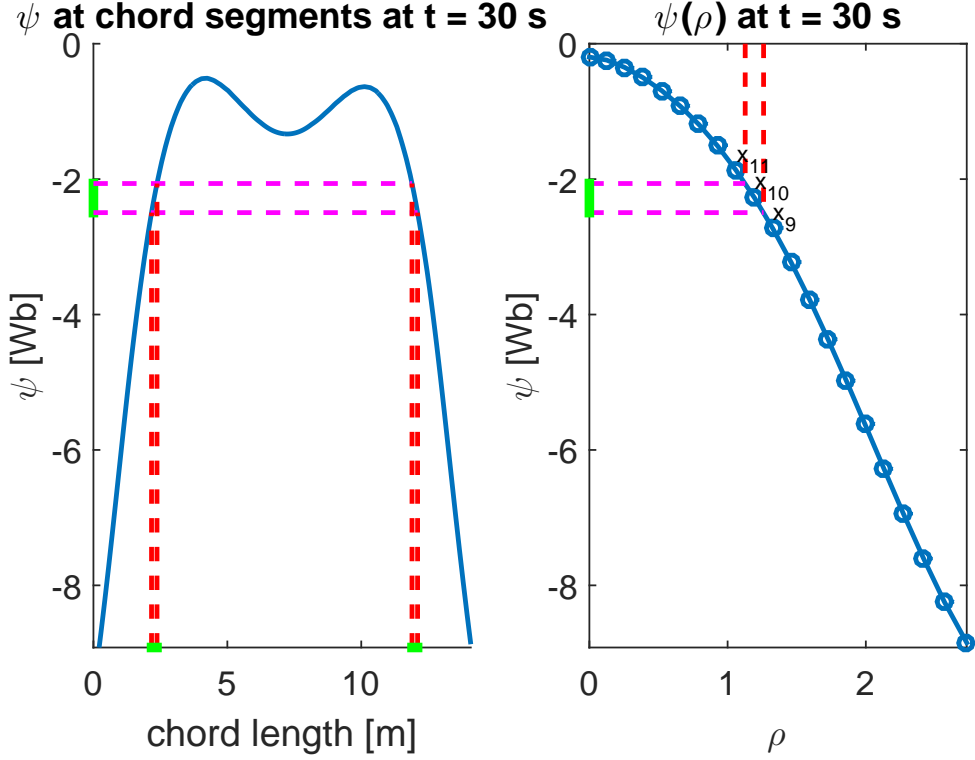


Figure 3.2: $\psi(\rho)$ in the right graph and ψ values for each part of the interferometer chord on the left. The midpoints between density points x_9 and x_{10} , and x_{10} and x_{11} are indicated by the dotted lines. The section of ψ values that corresponds to density point x_{10} , and the piece of the interferometer chord that lies between these flux surfaces and are indicated in green.

3.2.1 Derivative of electron density measurements with respect to the density state variable

For the observer, the synthetic diagnostic also needs to provide $\frac{\partial h}{\partial x}$, the derivative of the measurements with respect to the state variables x , which are used to parameterize the density profile, and are provided as input to the synthetic diagnostic. From equations 3.1, 3.2 and 3.3 the line-averaged measurement can be expressed as

$$n_{la} = \frac{\bar{\gamma}}{\bar{L}} \int_L \frac{n_e(\rho)}{\gamma(T_e(\rho))} dl, \quad (3.6)$$

with γ the Lorentz factor, L the total chord length and $\bar{\gamma}$ and \bar{L} the line-averaged quantities.

The input of the synthetic diagnostic is not a continuous function, but rather a discrete set of local densities at certain flux coordinates. As such equation 3.6 becomes

$$n_{la} = \frac{\bar{\gamma}}{\bar{L}} \sum_{i=1}^n \frac{n_{e,i}}{\gamma_i} L_i, \quad (3.7)$$

with i indicating the element of the discrete density grid. The derivative of the line average measurement with respect to the state variable x becomes

$$\frac{\delta n_{la}}{\delta x} = \frac{\bar{\gamma}}{\bar{L}} \left[\frac{L_1}{\gamma_1}, \frac{L_2}{\gamma_2}, \dots, \frac{L_n}{\gamma_n} \right] \Lambda, \quad (3.8)$$

with n the number of points in the density grid and Λ the matrix defining the relation between the state variable x and the discrete density grid n_e .

To calculate L_i in equation 3.8 the length of the chord passing through space with density $n_{e,i}$ must be found. The spatial position corresponding to a point on the density grid is defined by the normalized flux label ρ . Using a 2D flux map, $\psi(R, Z)$ along with the chord path the flux is plotted for each section of chord length, as seen in figure 3.2. The flux region corresponding to a point on the density grid i is defined and shown in figure 3.2. Using $\psi(l)$ and $\psi(i)$ the chord length L_i corresponding to a point on the density grid is calculated.

3.2.2 Concluding remarks

A model for the DI and TIP diagnostics is designed and implemented. An extension the model is presented to calculate the derivatives of the measurements with respect to the state variable provided as input, which is required for use with the observer model discussed in chapter 2.

Chapter 4

Control assesment

In this Chapter the results of the closed loop density simulations obtained during this project are discussed. First the reference plasma discharge used in the simulations is discussed and it is compared with the results obtained in previous work [15]. Furthermore, the tracking behavior of the control loop is assessed and the effect of including sensor models and the observer are presented. The influence of measurement errors on performance is discussed. The control performance over the full plasma discharge is discussed and the implementation in the PCSSP is discussed.

4.1 ITER D-T burning plasma discharge scenario

Because the RAPdens density model needs external input of the reference plasma parameters such as the plasma current and edge temperature, reference data for the discharge is required. The reference data is obtained from a CORSICA, an advanced free boundary transport simulation code, simulation [10]. The reference discharge simulates a D-T plasma. During the flattop phase alpha particle heating is present as a result of the D-T fusion reactions. The imporant transition in the shot is the forming of the x-point, where the plasma transitions from a limited to a diverted state. This transition occurs at about 11.5 seconds. The transition from L to H mode starts at 60 seconds when the NBI is turned on to heat the plasma. The transition takes about 15 seconds for the entire density profile. The plasma current ramp-up continues until it reaches 15 MA, the maximum for ITER. The flattop, during which the plasma parameters stay constant, lasts until 500 seconds at which point the current ramp down begins, causing the plasma electron density and volume to decrease with the current. At approximately 560 seconds the NBI is turned off and the plasma exits H-mode. While the plasma is in H-mode an edge transport barrier forms, reducing transport. This creates a pedestal in the density profile. When the plasma exits H-mode the pedestal disappears and the particles that make up the pedestal are lost, as can be seen in the drop in volume averaged electron density at 560 seconds. The shot is representative for one of the ITER H-mode scenario's. Some important parameters of the shot a given in figure 4.1

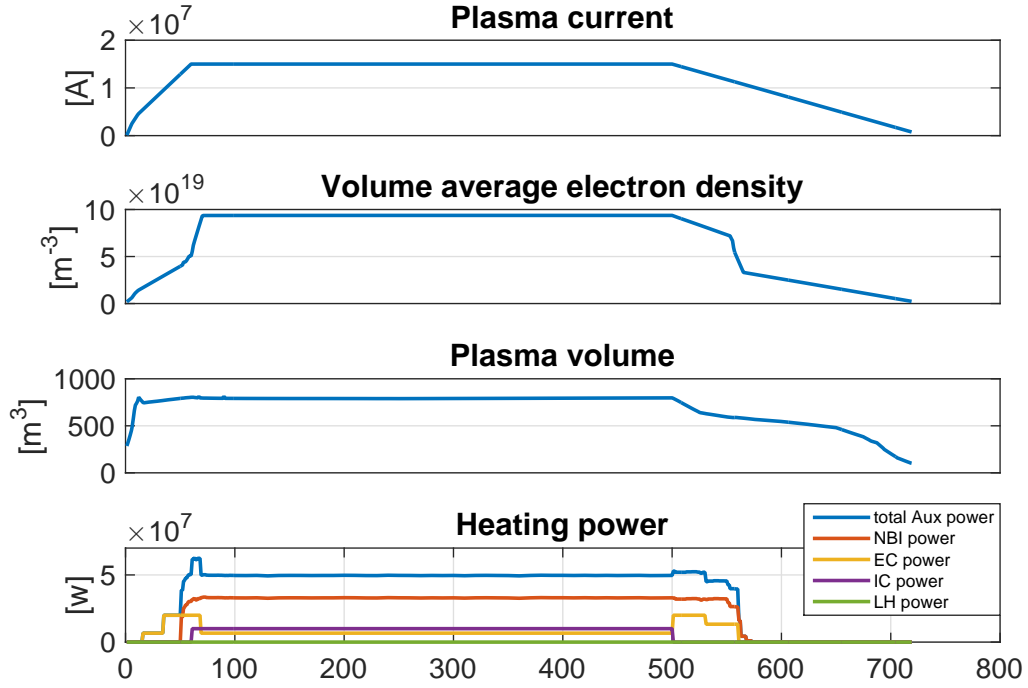


Figure 4.1: Parameters for the reference shot. During the flattop at $t = 300s$, $n_e = 9.410^{19}m^{-3}$, $V_p = 790m^3$, $I_p = 15MA$ and $P_{aux} = 50MW$.

4.2 Control performance comparison of plasma scenario with previous work

The new reference shot is compared with the results obtained in the previous density control work [15]. For this comparison the sensor and observer models are not included in order to match the previous work. The feedforward waveform is created for the new reference data set, and the model parameters are tuned for the new reference data. The reference density waveforms are obtained from their respective reference simulation.

As can be seen in figure 4.2 in both cases the open-loop simulated densities follow the reference and stay within the boundaries set as 90% and 20% of the greenwald density, $n_{gw} = \frac{I_p}{\pi a^2}$. The L-H transition begins at $t = 60s$ while the simulation in previous work lasted until $t = 50s$. Due to the different reference parameters, such as the current, the dynamical behaviour of the two simulations is different, but both track the density and remain within the stability boundaries.

The density of the new simulation rises at the end of the simulation due to the transition, which is not taken into account in previous work. ILC was applied for both reference discharges, using initial feedforward waveforms specific for both scenario's. The physics parameters were tuned for each reference discharge.

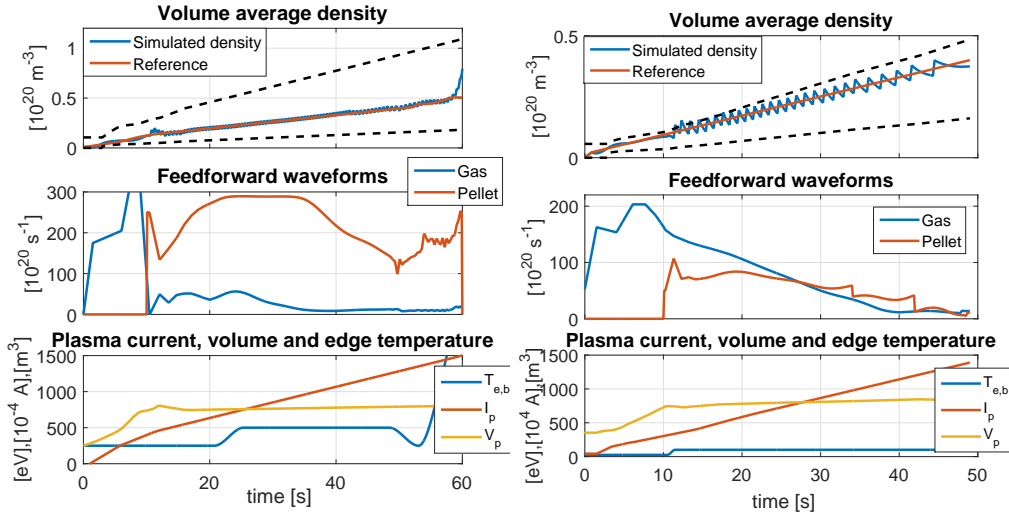


Figure 4.2: Comparison between results from open-loop simulations with new scenario (left) and results from previous work (right). Volume average electron densities are shown during ramp-up along with the reference trajectory and stability boundaries (90% and 20% of the greenwald density (dashed)).

4.3 Effects of including sensor and observer models

The diagnostic interferometer model and the state observer are introduced in the simulations. The feedforward waveform used the closed-loop simulations in this section are generated using 10 ILC iterations starting from a hand-tuned simple feed-forward and are optimized from $t = 0s$ to $t = 100s$, after which the feedforward waveforms are set to zero. The large pellets are used for the pellet injection. The feedback is set to use the gas injection up to $t = 10s$, after which pellet injection is used for feedback control. Measurements from the DI and TIP chords are used in the state observer.

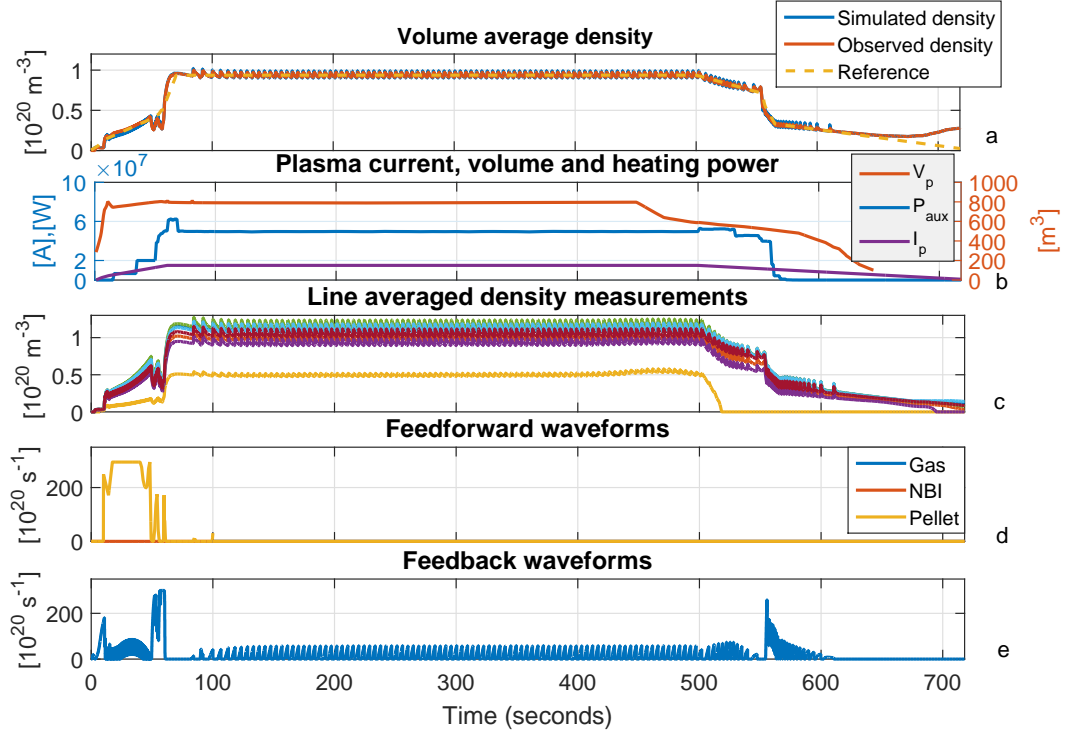


Figure 4.3: Simulation of the complete model with an ILC optimised feedforward using large pellets. The simulated volume average density is used in the feedback control. In panel a the simulated and observed volume average electron densities are shown with the reference. Panel b shows the I_p , V_p and P_{aux} of the reference simulation. Panel c shows the line averaged electron densities from the synthetic diagnostic for the 2 DI chords and the 5 TIP chords. Panel d shows the feedforward signals for gas, NBI and pellets optimized by the ILC. The Feedforward runs up to 100s because it is required during ramp-up. The signal for feedback control is used to inject gas up to 10 seconds after which it only uses pellet injection.

4.3.1 Full shot simulation with sensors and observer

In figure 4.3 the results of a closed-loop simulation are shown. In panel c the line-averaged electron densities are shown for both the DI and TIP chords. The TIP1 chord deviates from the other chords in that it fails to measure the density before the termination is completed. This is a results of the plasma shrinking and no longer intersecting with this chord's line of sight, as illustrated by figure 4.4 showing the shape and position of the plasma and the interferometer chords projected on the 2D cross section. It also has a lower measurement because it measures the density in the edge region of the plasma, which has the lowest density.

At the end of the simulation the density rises slightly instead of decaying to zero. This is possibly a result of the plasma volume going to 0 before the simulation has ended.

The interferometer model works as expected as the measured signals follow the volume averaged density. Slight differences can be seen as a result of H-mode where the existence of the pedestal in the density profile has more effect on the different chords depending on their intersection with this edge region of the plasma. This is most clearly visible between $t = 500s$ and $t = 550s$, where rampdown has started but the plasma remains in H-mode. The observer is able to accurately estimate the volume averaged density.

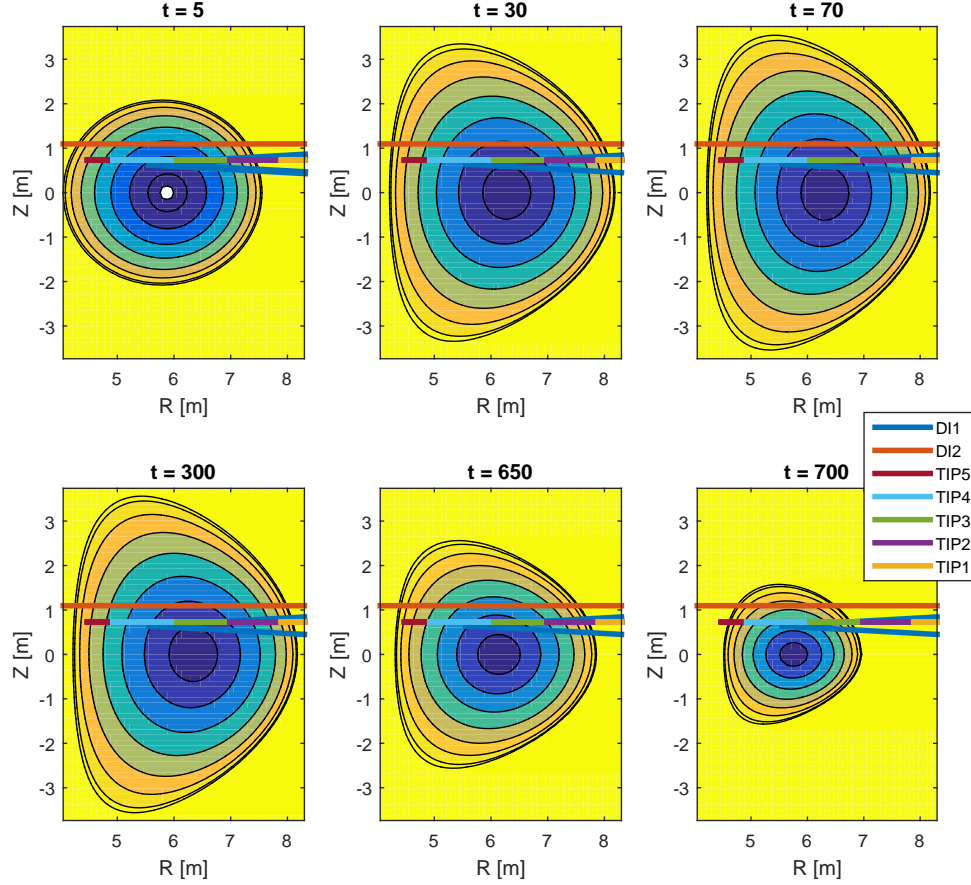


Figure 4.4: Cross section of the plasma at various times during the plasma discharge. At the beginning ($t = 5s$) the plasma is touching the wall (limited) and circular. After the formation of the X-point the plasma grows and becomes elongated and triangular. During the flattop phase the plasma maintains its shape ($t = 5s$) until the current rampdown starts. During rampdown the plasma slowly decreases in size and eventually slowly moves inward. Plotted in the figure are the lines of sight of the interferometer channels for the DI and TIP projected on the crosssection. The five TIP chords are horizontal at $z = 0.73m$ and overlap in the figure.

4.3.2 Simulation of measurement errors and effect on control

In diagnostic devices disturbances affect the measurement error. To simulate these errors a uniformly distributed noise with amplitude up to 1% and 10% of the measured signal amplitude is added to the measurements, corresponding to the tolerances on the diagnostics [3] [8].

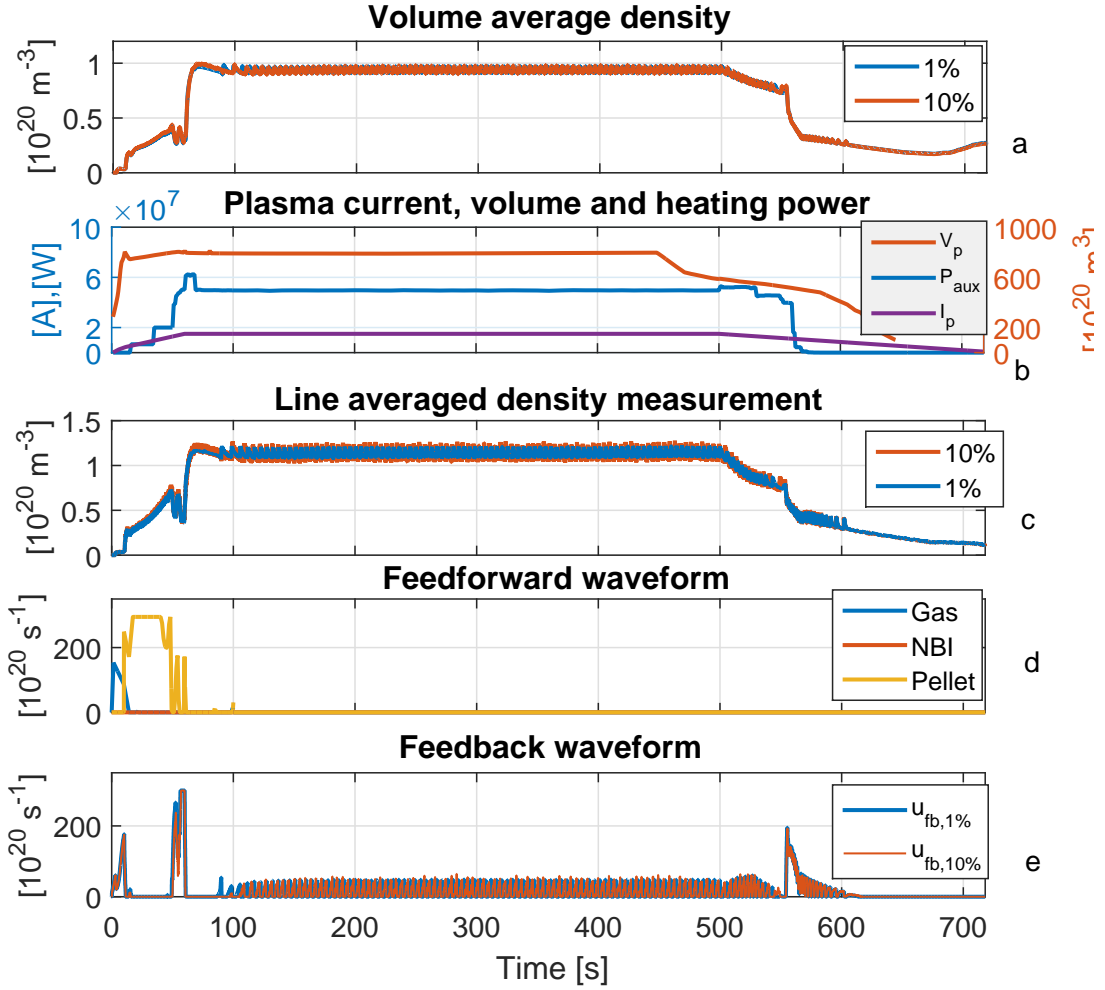


Figure 4.5: Two simulations of the complete model with an ILC optimised feedforward using large pellets. A uniformly distributed noise of 1 and 10 percent of the signal strength are added to each measurement chord. The observed volume average electron density is used in the feedback control. Panel c shows the line averaged electron densities from the synthetic diagnostic for the DI1 chord. Panel d shows the feedforward signals for gas, NBI and pellets optimized by the ILC. The Feedforward runs up to 100 s because it is required during ramp-up. The signal for feedback control for all three simulations is used to inject gas up to 10 seconds after which it only uses pellet injection.

In figure 4.5 the results are shown for simulations with noise added to the sensor models. Despite the noise being clearly visible on the line-averaged measurements, the volume averaged density estimated by the observer is not effected by the measurement noise. This indicates the observer is able to effectively reconstruct the density and is able to deal with the expected noise.

4.4 Control assessment results

In this section the use of ILC is investigated and its performance impact specifically around the L-H transition. It is important that the control error is small during the transition because a successful transition only happens if the density is at the right value.

4.4.1 Comparison of tracking with a simple feedforward and with ILC

First the need for ILC optimized feedforward is considered. In figure 4.6 a closed-loop simulation using a simple feedforward signal and a feedforward signal created with ILC are compared. The simple feedforward is hand-tuned. The ILC feedforward waveform used in the simulation is the result of 10 ILC iterations with the ILC running up to 100 seconds using the simple hand-tuned feedforward waveform as the initial feedforward waveform.

The simple feedforward waveform results in a much bigger overshoot. This as a result of the L-H transition where the increase in confinement causes the particles to remain longer in the plasma. The simple feedforward and the feedback controller cannot anticipate this change in dynamical behaviour resulting in excessive fuelling during ramp-up. This indicates the importance of having good feed-forward waveforms, which can be achieved using ILC.

4.4.2 Comparison of tracking during L-H transition for different ILC optimisation times

In previous work ILC was used to optimize the feedforward waveform during rampup. H-mode and with it the L-H transition was therefore not taken into account. When only optimizing the feedforward waveform during ramp-up, the transition point is not taken into account.

Five ILC waveforms are created for varying lengths of time. The shortest feedforward waveform is created for the first 60 seconds, when the transition to H-mode begins. The longest feedforward waveform is created for the first 100 seconds. The feedforward waveforms are set to zero for the remainder of the simulation.

In figure 4.7 the results of closed-loop simulations are shown for feedforward waveforms are shown. The shortest feedforward waveform perfectly tracks the reference during the first 60 seconds for which the feedforward is optimized. Despite lacking additional fuelling this simulation an overshoot of about 40%. This is a result of the improved confinement in H-mode.

The simulations with four longer waveforms do not show this overshoot, but instead have a lower density earlier during the ramp-up. This is a result of the difference in pellet feedforward waveforms.

The large overshoot is undesirable. This shows the importance of a properly tuned feedforward waveform, taking into account the transitions in the dynamics of the system.

4.4.3 Comparison of tracking during the L-H transition for different ILC costs

In the design of the ILC cost function a cost is present for errors around the time of the L-H transition. This cost was not used in previous work. In figure 4.8 results are shown from a closed-loop simulation including this cost with a weight of $W_{lh} = 10$ applied on the error from $t = 52$ to $t = 60$. The ILC waveforms are both created for the first 100 seconds of the simulation. The waveform for pellet feedforward for the case with the additional cost is overall lower, but this is negated by the increased feedback, resulting in near identical tracking during the first 40 seconds of ramp-up. As a result of the additional cost on the error right before the L-H transition, there is a better tracking during the that period compared to the normal waveform. The optimized feedforward does attempt to increase the gas fuelling at the beginning of this period above the

actuator limit, which is set to $200 \cdot 10^{20} s^{-1}$. The gas input during the simulation is capped so the excessive gas request is not delivered. The gas input does lower the need for feedback control at that time. This implies more gas delivery on the feedforward during this phase of ramp-up is desirable, which could be included in the initial feedforward waveforms for the ILC.

The tracking behaviour in the simulation with feedforward with the additional lh cost displays better tracking behaviour leading up to the L-H transition, which is to be expected. It also leads to a slightly higher overshoot after the transition. The inclusion of an additional cost on the error during critical points in the discharge can be a usefull tool to shape the feedforward waveform to get the desired behaviour.

4.4.4 Comparison of tracking during the L-H transition with different pellet sizes

The two main sizes for the fuelling pellets are $50 mm^3$ and $92 mm^3$. The effect of the smaller pellets on control is investigated. In figure 4.9 results from closed-loop simulations using the different pellets are shown. The performance of the small pellet is slightly better right after the transition. This is possibly an effect of more precise control as a result of smaller actuator steps. A notable difference between the feedback waveforms is the much larger feedback for small pellets resulting from the large error. This implies small pellet fuelling is less effective.

4.4.5 Ideal controller performance

In this section the control performance during the L-H transition is investigated. While the analysis is based on simple models, some observations are made on the desired control behavior of the density controller, specifically during this transition.

It is most important that the controller keeps the density within the stability boundaries. During most of the ramp up a larger error is not problematic, but during the moment of transition the error should be as small as possible. The controller should use small pellets to inject enough particles to stay as close below the reference as possible when approaching the L-H transition. It is important the moment of transition is predicted as precisely as possible

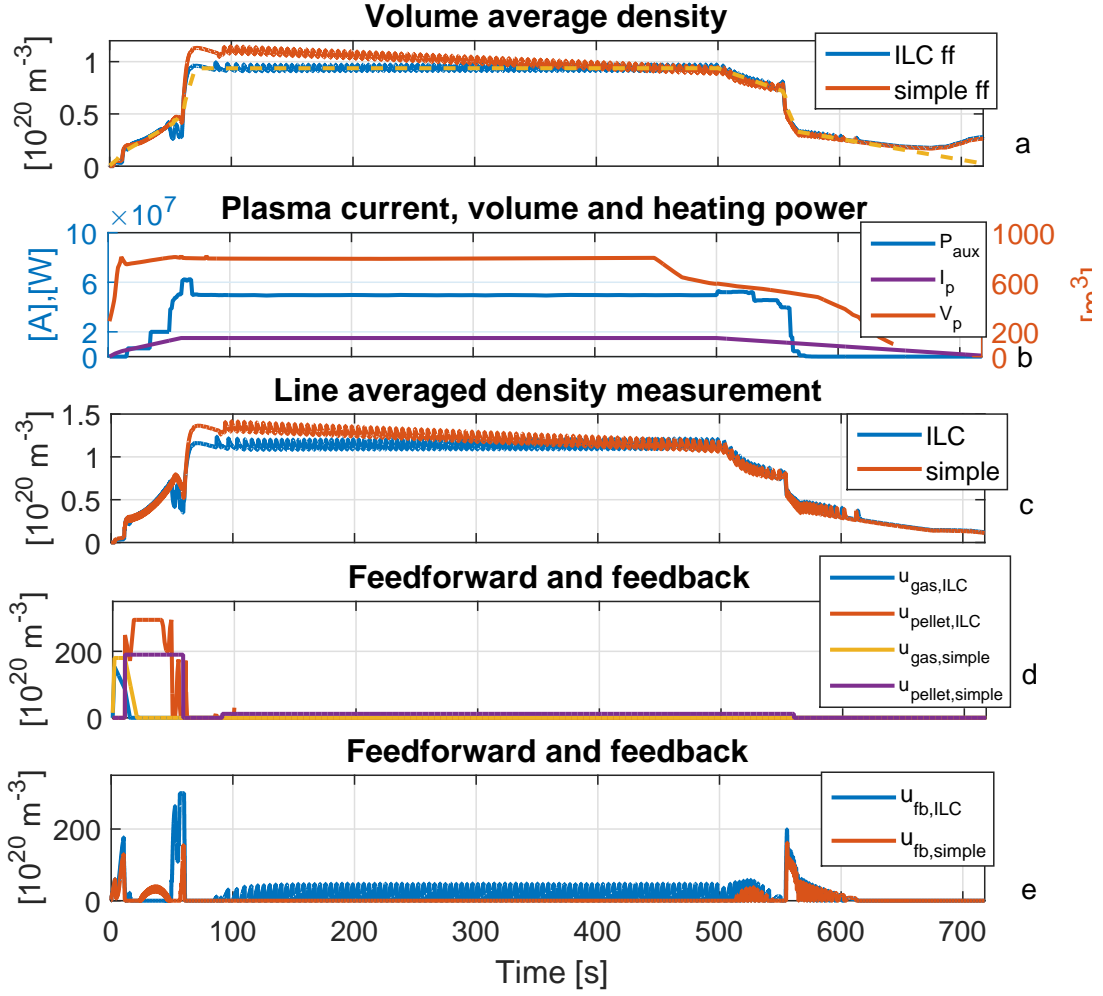


Figure 4.6: Two simulations of the complete model with an ILC optimised feedforward and a simple feedforward waveform using large pellets. The observed volume average electron density is used in the feedback control. In panel a the observed volume average electron densities are shown. Panel b shows the I_p , V_p and P_{aux} of the reference simulation. Panel c shows the line averaged electron densities from the synthetic diagnostic for the 2 DI chords and the 5 TIP chords for the optimised (continuous) and simple (dashed) feedforward waveform simulations. Panel d shows the feedforward signals for gas, NBI and pellets optimized by the ILC. The Feedforward runs up to 100s because it is required during ramp-up. The signal for feedback control for all three simulations is used to inject gas up to 10 seconds after which it only uses pellet injection.

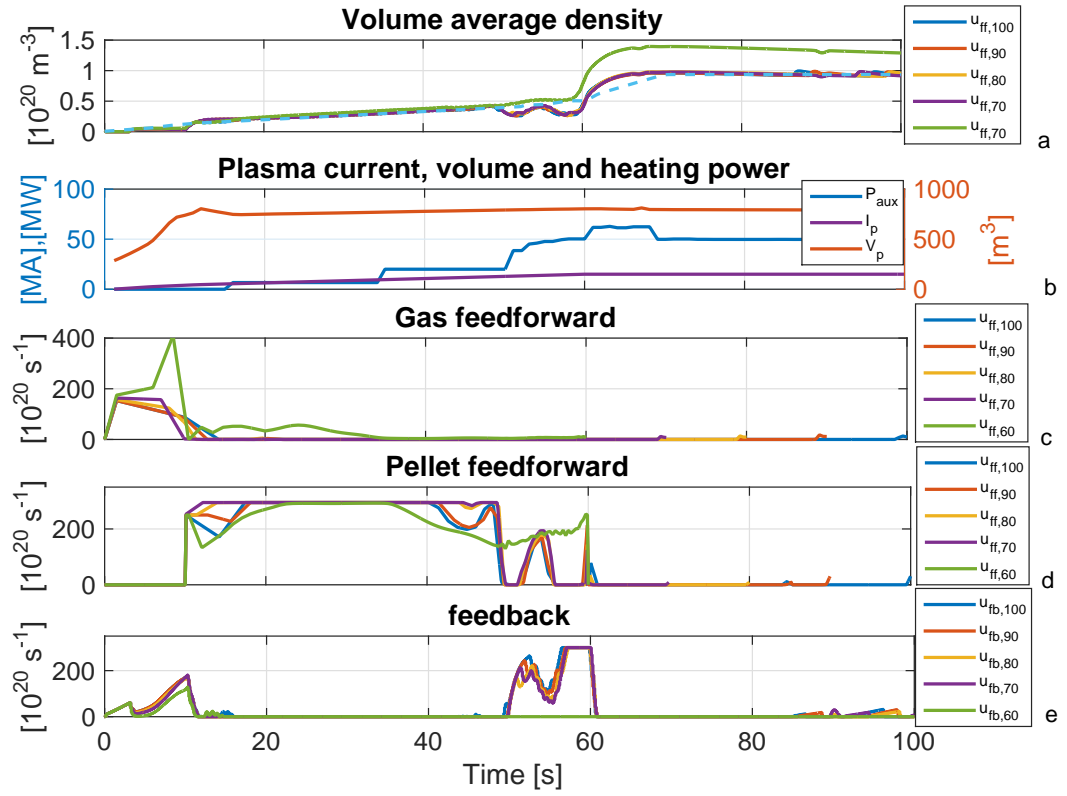


Figure 4.7: Five simulations of the complete model with feedforward waveforms optimised using ILC for different lengths of time using large pellets. The feedforward waveforms are optimised for a simulation of 60, 70, 80, 90 and 100 seconds. The observed volume average electron density is used in the feedback control. In panel a the observed volume average electron densities are shown. Panel b shows the I_p , V_p and P_{aux} of the reference simulation. Panel c shows the feedforward waveform for the gas injections for each simulation. Panel d shows the feedforward waveform for the pellet injection for each simulation. Panel e shows the feedback for the each simulation.

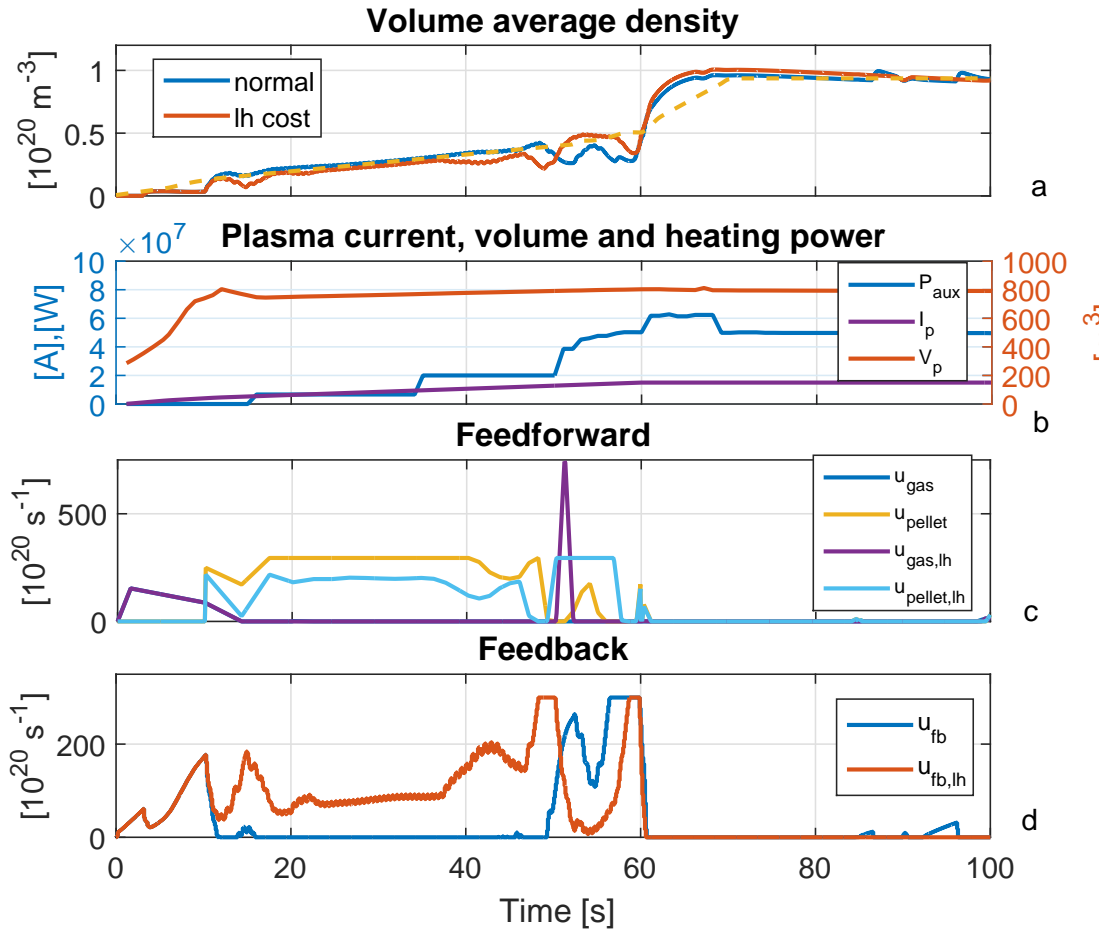


Figure 4.8: Two closed-loop simulations of the complete model with feedforward waveforms optimised using ILC with and without the additional cost during the LH transition using large pellets. The observed volume average electron density is used in the feedback control. In panel a the observed volume average electron densities are shown. Panel b shows the I_p , V_p and P_{aux} of the reference simulation. Panel c shows the feedforward waveforms. Panel d shows the feedback for the each simulation.

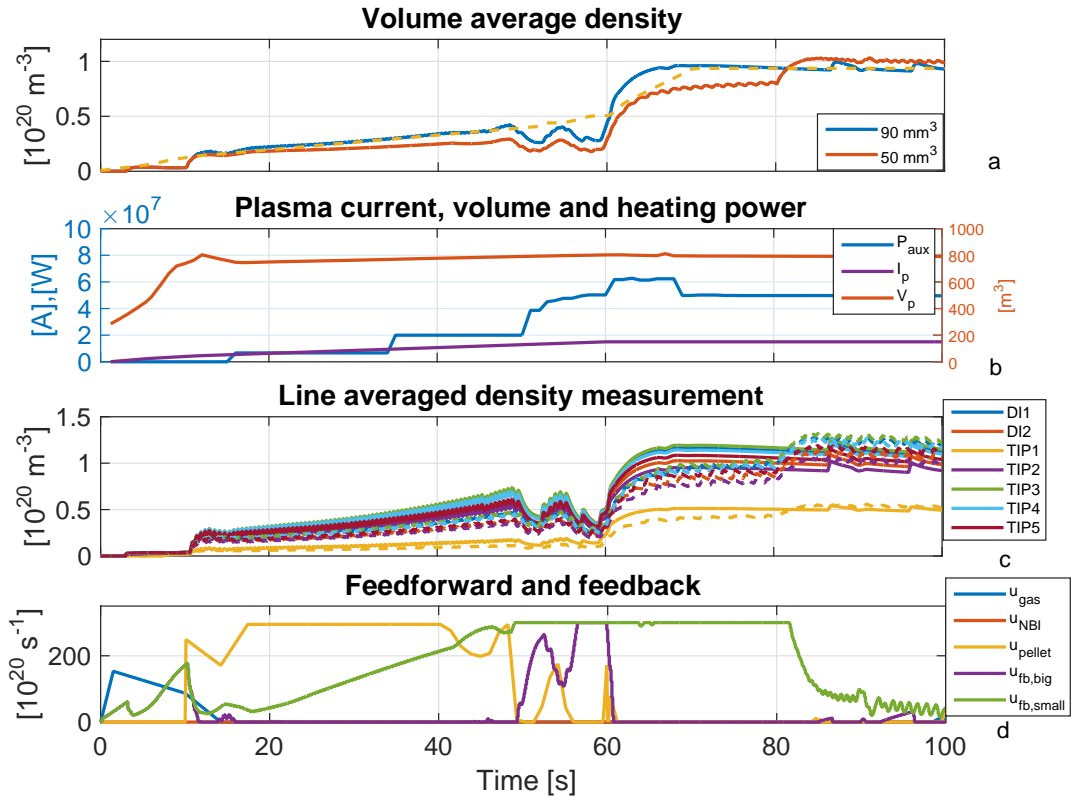


Figure 4.9: Two simulations of the complete model with feedforward waveforms optimised using ILC using large and small pellets. The observed volume average electron density is used in the feedback control. In panel a the observed volume average electron densities are shown. Panel b shows the I_p , V_p and P_{aux} of the reference simulation. Panel c shows the line averaged electron densities for the 2 DI and 5 TIP chords for the big pellet (continuous) and small pellet (dashed) simulations. Panel d shows the feedforward and feedback waveforms for the each simulation.

Chapter 5

Conclusions

In this chapter conclusions are drawn based on the results in chapter 4 and the research questions posed in the introduction are answered. These conclusions are then discussed and finally recommendations for the ITER density control and the future research are made.

5.1 Conclusions

To start the conclusions the problem statements from Chapter 1 are evaluated. The first research question is:

What is the effect of adding more complicated models for actuators, sensors, plasma physics and observers to the density control loop on controller performance?

In this work, models for sensors and observers were added to the closed loop simulations. In addition a model for the evolution of the plasma density was tuned to reproduce a full ITER H-mode discharge, including a reproduction of the confinement mode transitions.

Adding a sensor model to the closed loop system has a minimal influence on the performance during ramp-up and the flattop part of the shot. Adding a noise model to the sensor has a minor impact on the error. This shows the state observer is capable of dealing with these errors and ensures this is not an issue for the control.

An extended kalman filter based observer is added to the model, which takes the line-integrated density measurements as input along with the actuator inputs and plasma parameters required for the density model and reconstructs the density. This addition compensates for the noise and results in good tracking behavior.

Overall the addition of more complex models results in slightly worse performance though this is compensated for by the addition of a state observer.

The second research question is:

What is the best achievable performance of the density control loop in terms of reference tracking?

Using the tools developed during this project the performance is evaluated. Using the full loop and the full ITER shot, the best performance is achieved using a hybrid control scheme and a feedforward waveform for the gas and pellet injection computed over a full shot.

The third research question is:

Is the framework of IMAS and PCSSP adequate for closed-loop density simulations of ITER?

During this project the models for density control are adapted to fit into the PCSSP framework and this framework is used to complete the simulations. As such the PCSSP offers an adequate framework to conduct closed-loop density control simulations in.

5.2 Discussion and outlook

In this sections the used models, sensors and defects are discussed as well as some of the underlying assumptions in the use of the observer.

5.2.1 Sensors

In this project a model for the dispersion interferometer system on ITER is introduced into the control loop. This model calculates the refractive index and resulting phase and represents the physical system. The model is however still very simple and does not contain any advanced dynamics present in such interferometer systems. Therefore only limited conclusions can be drawn based on the use of this model.

One of the main concerns for density control systems is the presence of fringe jumps in the interferometry measurements. The ITER DI and TIP, which will be used for the density control, are designed not to have fringe jumps. Hence this common issue is not discussed in this work.

A simple random measurement error is included in the sensor models. This is however not a complete and representative description of the potential errors on sensor and interferometry systems. It is therefore important to note that any conclusion on the performance of control based on current simulations might not be representative for reality, and further modelling of sensor defects should be included in future work. These errors can include sensor failure, fringe jumps and other systematic errors.

5.2.2 Parameters

The density evolution model used this project is the RAPdens model. Since it is a control oriented 1-D model it contains only a simplified set of dynamics. The model parameters for this model are chosen to match empirical data. Because ITER is not operational yet, there are no experimental results for the device, and because there are no other devices like it, it is impossible to know what the empirical results for ITER will look like. As such there is a large uncertainty in the device parameters. Therefore any conclusions based on the current simulations are subject to the same uncertainties and therefore no hard conclusions can be drawn on the control. It is important that systematic tools are created to do these control analyses as more realistic information becomes available.

The current parameters are chosen such that the L- and H-mode density profiles match the expected profiles based on experience with current day devices.

5.2.3 Observer and feedforward model mismatch

The RAPdens density model which is used as the density simulator for this project is designed to be used in the real-time density observer which is also introduced into the loop. Because of this, the same density model is used to evolve the density and to estimate the evolution. As with any causal system, given the same input, the resulting output will be identical and as such any conclusion about the performance of the observer is not representative for when the observer is used on the real system, which behaves differently from the RAPdens model.

To avoid this bias, a model mismatch is introduced between the RAPdens models which are used for the simulation and in the observer. This mismatch is made by slightly changing some of the parameters. To help alleviate the bias entirely, a different model should be used to simulate the density evolution. At the time of this project, no other density simulator was made available but in future, potentially with the integration of IMAS codes for PCSSP, this should be done.

5.2.4 ITER reference plasma discharge

The RAPdens density simulator requires additional input information about the plasma parameters. This information includes plasma current, plasma volume and the mode, H- or L-mode, of the system among other things. Whereas in real-time this information could be provided by other control systems, for these density simulations the information is provided externally. This information is obtained from a CORSICA simulation. Because this information is obtained in another simulation the evolution of the density simulation might not be consistent with the evolution of the other parameters. Therefore whenever there is a large difference between the reference density, obtained from the density in the CORSICA simulation, the reliability of the results decreases. To solve this issue the density evolution should ideally come from a single full plasma simulator, or at least be run in a larger simulation in which the density is fed back into the other plasma simulators to ensure the consistency of the results.

Also, in part because the operation of the ITER system is still unknown, the data from the CORSICA simulation is subject to its own errors and uncertainties. These errors propagate in the density simulations that use this data.

5.3 Future work

In this section some ideas for future work are discussed and recommendations are made.

5.3.1 Sensor models

In this project only the DI and TIP are modelled and added to the system. These are only two of the density measurements available on ITER. Adding models for the other diagnostic, such as a Thomson scattering diagnostic, allows for research on the density control performance using these other diagnostics as well as research into the effect of using multiple different diagnostics.

Furthermore, the errors of these diagnostics need to be modelled in greater details as this is highly relevant for control performance. This is also the case for the dispersion interferometer model which is currently used. For this more complex and realistic physics and models need to be included.

In addition to the relativistic effects on the electron mass, finite thermal effects can increase the electron plasma frequency [9]

5.3.2 Termination scenario's

In this project the density evolution is considered during the entire shot, as opposed to only during ramp-up. The termination phase is however a particular case. Comparatively little research has been done on this phase since it requires no special attention for smaller machines. Because of this the used termination phase is not well substantiated. Therefore it might be beneficial to devote special attention to modelling a realistic ramp-down and termination phase for the density control and specify the controller requirements during that phase. Research on rampdown optimization is being done at TCV [19] and DII-D [12] [2].

5.3.3 Hybrid control

As determined in a previous project on the ITER density control simulations, it was concluded that feedforward control was needed to compensate for slow actuators during ramp-up. When looking at the full shot performance, it becomes apparent that the requirements for feedback control during the ramp-up, flat-top and ramp-down phases of ITER operation are different. A high gain controller during ramp-up can result in severe overshoot when entering H-mode due to the input effort of the feedforward. A low gain controller during the flat-top regime might not be able to keep the density at the steady state reference. As such during this project the controller gain is switched between these phases, essentially making it a hybrid controller.

However little research is done on this topic. More research is warranted on the consequence of different controllers for different phases of ITER operation. Multiple schemes such as hybrid or adaptive gain control can be investigated to find optimal performance for the system.

5.3.4 Profile and mixed species control

Current control simulations in this density control project are being done where the controlled variable is the volume average electron density. Considering the density profile is observable using other density diagnostics and the equilibrium solvers, and considering different density actuators, gas, small pellets and larger pellets, have different fuelling positions, the density control could be used in the profile control.

In reality the device will run on a deuterium tritium mixture. Because the mixture of both species is important, especially in the center, this could also be considered as a control variable. This would require an expansion of the density model so that it is capable of tracking multiple ion species.

Bibliography

- [1] Simulink 8.5 (r2015a). 2
- [2] Politzer P A. Experimental simulation of iter rampdown in diii-d. *Nuclear Fusion*, 2010. 31
- [3] Sirinelli A. System design description (ddd) 55.fa density interferometer polarimeter (dip). Technical Report E6CMPD, ITER organisation, 2016. 13, 22
- [4] Snipes J A. Physics of the conceptual design of the iter plasma control system. *Fusion Engineering and Design*, 2014. 2
- [5] Pégourié B. Recent results on the fuelling and control of plasmas by pellet injection, application to iter. *Plasma Phys. Control. Fusion*, 2009. 9
- [6] Blanken T C. Model-based reconstruction and control of the density in tokamaks. Master's thesis, Eindhoven university of technology, 2014. 5, 8
- [7] Blanken T C. Control-oriented modeling of the plasma particle density in tokamaks and application to real-time density profile reconstruction. *Plasma Physics and Controlled Fusion*, 2017. 7, 11, 12
- [8] Watts C. 55.c5 ddd of the toroidal interferometer/polarimeter(tip). Technical Report 64DPDP, ITER organisation, 2012. 13, 22
- [9] Brower D L et al. Advanced interferometry techniques for burning plasmas. In *AIP Conference Proceedings 988*, 2008. 31
- [10] Kim S H. Simulating burning plasma operation in iter, 2014. 42e EPS Conference. 17
- [11] F. Imbeaux, S.D. Pinches, J.B. Lister, Y. Buravand, T. Casper, B. Duval, B. Guillerminet, M. Hosokawa, W. Houlberg, P. Huynh, S.H. Kim, G. Manduchi, M. Owsiak, B. Palak, M. Plociennik, G. Rouault, O. Sauter, and P. Strand. Design and first applications of the iter integrated modelling & analysis suite. *Nuclear Fusion*, 55(12):123006, 2015. 35
- [12] Jackson G L. Simulating iter plasma startup and rampdown scenarios in the diii-d tokamak. *Nuclear fusion*, 2009. 31
- [13] Walker M L. A simulation environment for iter pcs development. *Fusion Engineering and Design*, 2014. 2
- [14] Anderson B D O. *Optimal filtering*. Prentice-Hall, Inc., 1979. 11
- [15] Timo Ravensbergen, Peter C de Vries, Federico Felici, Thomas Cornelis Blanken, Remy Nouailletas, and L Zabeo. Density control in iter: an iterative learning control and robust control approach. *Nuclear Fusion*, 2017. 3, 9, 10, 11, 17, 19
- [16] Maruyama S. Srd-18-pi (pellet injection) from doors. Technical Report 2AB6D3, ITER organisation, 2013. 6, 9

- [17] Pinches S. The iter integrated modelling programme. Technical Report 2ERF4K, 2014. 2
- [18] Ravensbergen T. Advanced control of iter plasma density. Master's thesis, Eindhoven university of technology, 2016.
- [19] A A Teplukhina. Simulation of profile evolution from ramp-up to ramp-down and optimization of tokamak plasma termination with the raptor code. *Plasma Phys. Control. Fusion*, 2017. 31
- [20] Bristow D Tharayil M and Alleyne A. A survey of iterative learning control". *Control systems IEEE*, pages 96–114, 2006. 10

Appendix A

In this project the simulations are done using the PCSSP. Remarks on use of the PCSSP, as the first user, are presented here. Additionally, an integration between PCSSP and IMAS is proposed.

5.4 Using PCSSP

This project is one of the first to use the PCSSP since its development. As a test user it is inevitable to encounter issues. Steps can be made to improve the user-friendliness of the platform, specifically with regards to its installation. While the documentation is complete some clarity could be added, specifically in regard to limitations it imposes in the models used in PCSSP simulations and its modules. Some of the limitations are a consequence of its data structuring and are as such not initially apparent. As a framework built in simulink the PCSSP imposes a few additional restrictions on what is allowed in module construction. As a result of these combined restrictions the implication for module design are not always apparent. Restrictions to what is allowed as a result of using the PCSSP framework, direct or resulting of the interaction with the simulink restrictions, should be explicitly noted.

5.5 Linking PCSSP and IMAS

The added benefit of the PCSSP is tied to the size of its module repository as most of the additions PCSSP makes to the Simulink environment are focussed on easily swapping modules between simulations. To evaluate this use of the PCSSP, its module library needs to be expanded. A coupling between the IMAS and PCSSP systems could therefore benefit both platforms as a link could effectively include the IMAS codes to the PCSSP module repository. A first step for this could be the creation of a generic S-function to wrap around IMAS codes written in C, C++ or fortran so they can be used in PCSSP simulations.

To further the integration, links with the IMAS repository, and importing and storing PCSSP data in the IMAS data format are to be made. For this integration it might be helpful to define the desired users and use-cases for both platforms and their overlap, and in what capacity either platform needs to be used for the integration with the other platform to be functional.

A functional link between the PCSSP and IMAS has been considered previously [11], using external workflow managers to run the IMAS codes. This solution has not been implemented. An alternative integration scheme is proposed here through the use of an S-function to have the entire simulation in Simulink®. The S-function wrapper should take the incoming PCSSP signals and, using the IDS definition and the module configuration, place the incoming signals in their place in the IDS's it generates and feed those to the IMAS code. The IMAS code is called and relevant control signals are automatically extracted from the output IDS's and fed back into the PCSSP. In the interest of doing controller development it is important that simulation are fast and easy to adapt and tune. Therefore it is undesirable to use the IMAS IDS's in the PCSSP simulation, as they contain more data than is necessary for individual simulations.

Potential issues in linking PCSSP and IMAS are:

- IMAS IDS's contain much more information than is desirable in control simulations. Isolating the relevant signals for control should be automatable.
- The availability of PCSSP and IMAS is not shared on all platforms, potentially limiting the user base.
- The IMAS IDS definition for MATLAB[®] contain cell objects, which are not compatible with Simulink simulations.